Numerical simulation of transient flow with column separation using the lattice Boltzmann method

Kai Wu, Yujie Feng, Ying Xu

Numerical simulation of transient flow with column separation using the lattice Boltzmann method

Kai Wu and Yujie Feng*

State Key Laboratory of Urban Water Resource and Environment,
School of Environment,
Harbin Institute of Technology,
No. 73, Huanghe Road, Harbin, Heilongjiang, China
Email: kawu01@hotmail.com
Email: yujief@hit.edu.cn
*Corresponding author

Ying Xu

School of Energy and Architecture Engineering,
Harbin University of Commerce,
No. 1 Xuehai Street, Harbin, Heilongjiang, China
Email: joexying@126.com

Abstract: This study proposes a numerical solution to simulate the transient flow with column separation in pipelines using the lattice Boltzmann method (LBM). By combining the LBM and the discrete vapour cavity model (DVCM), the governing equations and boundary conditions were analysed and derived for numerical simulation. Experiments and actual projects were adopted to verify and examine the new solution. The results indicate that the computational grid of the LBM-DVCM is unrelated to the wave speed, which significantly reduces computational resources and time. Moreover, compared to the method of characteristics (MOC)-DVCM, the LBM-DVCM eliminates virtual pressure peaks during the transient flow. Finally, the LBM-DVCM can simulate the process of transient flow quickly and accurately. It is expected that this method will be useful for practical numerical experimentation and efficient prediction of the pipeline.

Biographical notes: Kai Wu is a PhD candidate in the School of Environment, Harbin Institute of Technology, China. He received his Master's in Environmental Engineering from the Universität Stuttgart of Germany in 2006. His research interests include transient flow analysis of pressurised pipeline, drainage engineering, sewage treatment technology, solid waste treatment technology and environmental chemistry.

Yujie Feng is a Professor in the State Key Laboratory of Urban Water Resource and Environment, Harbin Institute of Technology, China. She obtained her PhD in Environmental Engineering from the Harbin Institute of Technology in 1996. She received her Postdoctoral degree from the University of Hongkong in 1999. Since 2018, she is the Dean of School of Environment in the Harbin Institute of Technology. Her main areas of research interest are research, development and application of functional materials in pollution prevention and environmental biotechnology.

Ying Xu is a Professor in the School of Energy and Architecture Engineering, Harbin University of Commerce, China. She obtained her PhD in Heating, Gas, Ventilationing and Air Conditioning Engineering from the Harbin Institute of Technology in 2009. She received her Postdoctoral degree from the Harbin Institute of Technology in 2011. Her main areas of research interest are transient flow analysis of pressurised pipeline, engineering applications of computational fluid dynamics and renewable energy utilisation.

1   Introduction

Liquid column separation and vapour cavities accompany hydraulic transient flow in pipelines when the transient pressure temporarily drops to the vapour pressure of the liquid at a certain temperature (Wylie, 1992). These vapour cavities appear at specific locations, such as high points (Simpson and Wylie, 1993). The collapse of these cavities in a pipe can generate high-pressure peaks instantaneously, which are stronger than the Joukowsky pressure (Bergant and Simpson, 1999). If this phenomenon occurs repeatedly, it might destroy the pipeline systems dramatically (Bergant et al., 2006). Long-distance water supply pipelines may have many more cavities owing to the long and complex topography (Zhou et al., 2018). To describe and understand this phenomenon in more detail, a series of numerical studies have been conducted on column separation in pressurised pipes (Bergant et al., 2006; Sadafi et al., 2012; Stewart et al., 2018). Among these studies, the discrete vapour cavity model (DVCM), which considers these cavities as internal and end boundaries, is a relatively simple numerical model and easy to be solved. Hence, the DVCM is widely used combined with numerical methods, particularly the method of characteristics (MOC) (Wylie, 1985). The MOC is easy to code, relevantly accurate, and efficient. Nevertheless, Santoro et al. (2018) demonstrated that the MOC had some disadvantages in practical applications. There are virtual pressure peaks in the MOC-based numerical simulation. A simulation of long distance pipes has a large number of computational points, which can significantly affect the efficiency of the MOC. Although the practice of the MOC-DVCM is confirmed to be easy to code with acceptable accuracy on the experimental scale, the drawbacks of the MOC became increasingly obvious in later practical applications (Gao et al., 2018). This may be because the spatial disposition of simulation nodes is limited and fixed in specific conditions. For example, the distance between two inner boundary conditions, such as two vapour chambers, may change as transient flow occurs, but the node spacing is fixed in the whole system. Consequently, a long pipe section can impose a large number of computational points. In fact, spatial or time interpolation can be used, but additional complicated procedures and inaccurate methods are required (Budinski, 2016; Zhang et al., 2018). To overcome these shortcomings, Cheng (1998) introduced the lattice Boltzmann method (LBM) as an alternative approach.

The LBM was developed from the lattice gas automata (LGA). Owing to the use of Boolean variables, the LGA model does not encounter numerical instability problems (Hoogerbrugge and Koelman, 1992). Moreover, the collision and flow of all particles occur simultaneously, and the interaction between particles is partial. It is suitable and convenient to implement on computers when dealing with complex boundaries, such as fluid particles bouncing back into the field at the boundary of a solid wall; however, the calculation results fluctuate significantly as the LGA only performs integer operations between 0 and 1. To decrease the computational cost, the integer operation in the LGA was changed into a real number operation, and a Boltzmann grid model was established to overcome the shortcomings of numerical noise in the LGA. To simplify the above model, a linearised collision operator model was proposed. This model introduces the equilibrium distribution function f_i^{eq} to linearise the collision operator $\Omega_i(f) = K_{ij}(f_j - f_i^{(eq)})$, where $K_{ij} = \partial\Omega_i / \partial f_j$ is called the collision matrix. From a numerical point of view, this linearisation process simplifies the calculation and significantly reduces the storage capacity. However, the numerical stability of this method is poor. A Boltzmann grid model of the reinforcement operator was further proposed. The collision matrix of the model is an asymmetric circular matrix, and its elements are only related to the included angle of discrete velocity. Based on it, some researchers proposed a simpler model, the single relaxation model. In this model, the collision process is replaced by a relaxation process that tends to a certain equilibrium state, and the matrix is determined by a parameter called relaxation time $K_{ij} = -(1/\tau)\delta_{ij}$ (Zou and He, 1997).

In fluid mechanics problems, the evolution of the LBM is the distribution function, and the distribution function on the boundary is unknown. Therefore, certain formats need to be constructed to obtain the distribution function. The boundary conditions affect the accuracy of the calculation results and influence the stability of the calculation. Cheng et al.(1998) proposed a general boundary processing method assuming that the unknown distribution function and the equilibrium distribution function have similar forms: $f_\alpha = \omega_\alpha\rho \left[1 + 3e_\alpha(u_w + s)\right]$ $\alpha = w \rightarrow b$, where ρ is the assumed density, u_w the is boundary speed, s the is assumed slip speed relative to the boundary, and the term of $w \rightarrow b$ indicates the direction from the outside of the boundary to the boundary (Budinski, 2016; Cheng et al., 1998). The advantage is that it can solve any number of unknown distribution functions, and it has good generality. It overcomes the shortcomings of other methods that can only solve a limited number of unknown distribution functions. Later, a processing method applicable to any curved boundary was proposed (Filippova and Hanel, 1998). Linear interpolation is performed using a known distribution function near the edge and wall to solve the unknown distribution function at the boundary. The velocity on the boundary is also solved using linear interpolation. However, this method requires a lot of calculations.

Recently, because of the reduced computational costs, some pieces of research have used this method to simulate the single-phase transient flow in pipelines; however, no simulation and analysis of two-phase transient flow was performed using the LBM (Budinski, 2016). Therefore, in this paper, the LBM combined with the DVCM was considered to simulate two-phase transient flow. First, the LBM-DVCM was proposed, including the control equations and boundary conditions. Then, experimental results were used to verify the new method in the classical reservoir pipe-valve system (Bergant and Simpson, 1999). In addition, the MOC-DVCM and LBM-DVCM were

compared. Finally, the effectiveness of the LBM-DVCM was compared to that of the MOC-DVCM based on a practical long-distance water supply system.

2 Method

2.1 Transient flow equations

The wave speed is significantly higher than the fluid velocity. Hence, the continuity equation and motion equation of one-dimensional transient flow can be simplified as follows (Zhou et al., 2017):

$$\frac{\partial H}{\partial t} + \frac{a^2}{g}\frac{\partial V}{\partial x} = 0, \tag{1}$$

$$\frac{\partial V}{\partial t} + g\frac{\partial H}{\partial x} + \frac{\mu}{2D}V|V| = 0, \tag{2}$$

where H is the piezometric head, x is the spatial coordinate, g is the gravitational acceleration, V is the fluid (mixture) velocity, t is the time, and μ is the friction factor. The wave speed a is defined as:

$$a^2 = \frac{K/\rho}{1 + \frac{K \cdot D}{E \cdot e}} \tag{3}$$

where K is the bulk modulus of water, ρ is the density of water, E is the elastic modulus of the pipe wall material, and e is the thickness of the pipe wall.

In this study, the two-phase transient flow is studied using the D1Q3 LBM (Frisch et al., 1986), and the three-velocity lattices are $\{e_2, e_0, e_1\} = \{-1, 0, 1\}$, as shown in Figure 1.

Figure 1 Boltzmann D1Q3 model
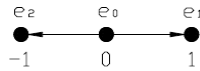
The local equilibrium distribution function can be expressed as:

$$f_i(x + e_i\Delta t, t + \Delta t) = f_i(x, t) + \Omega_i(f) \tag{4}$$

where f_i is the particle distribution function along the i link, x is the position vector in the one-dimensional domain, and Δt is the time step. The three-velocity lattice particles e_i along the x direction are defined as $e_0 = 0$, $e_1 = \Delta x/\Delta t$, and $e_2 = -\Delta x/\Delta t$. $\Omega_i(f)$ is the collision term.

For non-equilibrium systems, the distribution function of a molecule is a function of spatial position x, velocity v, and time t, that is, $f(x, v, t)$. According to statistical mechanics (Chen and Doolen, 1998), f obeys the equation

$$\frac{\partial f}{\partial t} + v\frac{\partial f}{\partial x} + \frac{F}{m}\frac{\partial f}{\partial v} = \Omega(f) \tag{5}$$

where F is an external force, and m is the molecular mass collision term given by:

$$\Omega(f) = \frac{1}{\tau_0}\left[f(x, v, t) - f^{(0)}(x, v, t).\right] \tag{6}$$

$f^{(0)}(x, v, t)$ is the Maxwell-Boltzmann equilibrium distribution function, and τ_0 is the relaxation time. The collision term means that the amount of change in the distribution function caused by each collision is directly proportional to the amount of deviation from the local equilibrium state; thus, $\omega = 1/\tau_0$ is also called the collision frequency.

According to equations (5) and (6), a continuous equation without external force term can be obtained as follows.

$$\frac{\partial f}{\partial t} + v\nabla f = -\frac{1}{\tau_0}\left(f - f^{(0)}\right) \tag{7}$$

$$\rho = \int fdv, \quad \rho u = \int vfdv. \tag{8}$$

When performing numerical calculations, it is necessary to perform numerical integration on equation (8). The following numerical integration form is applied:

$$\begin{aligned}\rho(x, t) &= \sum_i w_i f(x, e_i, t)\\ \rho u(x, t) &= \sum_i w_i e_i f(x, e_i, t)\end{aligned} \tag{9}$$

where e_i and w_i are the weight coefficients of the discrete velocity and numerical integration formulas, respectively, and the specific form is determined by the selected numerical integration method.

According to equation (7), the evolution equation can be derived as follows.

$$\frac{\partial f_1}{\partial t} + e_i\nabla f_i = -\frac{1}{\tau_0}\left(f_i - f_i^{(0)}\right) \tag{10}$$

Equation (10) is discretised into a finite difference scheme as follows

$$f_{\rightarrow}(x + e_i\Delta t, t + \Delta t) - f_i(x, t) = -\frac{1}{\tau}\left[f_i(x, t) - f_i^{(0)}(x, t)\right] \tag{11}$$

where $\tau = \tau_0/\Delta t$ is the dimensionless relaxation time. In this study, the Maxwell-Boltzmann equilibrium distribution function $f^{(0)}(x, v, t)$ is

$$f^{(0)} = \frac{1}{\exp\left(A + Bv \cdot u + C|v|^2\right)}. \tag{12}$$

The terms A, B and C are Lagrange's undetermined coefficients, which are a function of density and temperature (Al-Neama et al., 2017).

Under the condition of low Mach number, $|u|$ is very low and is expanded to the power series of $|u|^2$ the equation $f^{(0)}(x, v, t)$ is expanded by Taylor series, and the basic form of the equilibrium distribution function in statistical mechanics is obtained:

$$f^{(0)}(v) = C_0 + C_1 v \cdot u + C_2 (v \cdot u)^2 + C_3 |u|^2 + C_4 (v \cdot u)^3 \\ + C_5 (v \cdot u) |u|^2 + \cdots \tag{13}$$

where $C_k = (k = 1, 2, \cdots)$ are undetermined constants. Similar to equation (13), the equilibrium distribution function of the Boltzmann grid method can take the following general form (Cheng et al., 1998).

$$f_i^{(0)} = C_{i0} + C_{i1} (e_i \cdot u) + C_{i2} (e_i \cdot u)^2 + C_{i3} |u|^2 \\ + C_{i4} (e_i \cdot u)^3 + C_{i5} (e_i \cdot u)^2 |u|^2 + \cdots \tag{14}$$

Similarly, C_{i0}, C_{i1}, C_{i2}, C_{i3}, C_{i4}, C_{i5} are the undetermined constants.

The Chapman-Enskog (CE) expansion and multiscale analysis are used to connect Boltzmann grid equations and macrophysical equations. The local equilibrium distribution function in the Boltzmann grid equation must be determined by comparing the multiscale equation with the specific physical equation (Wolf-Gladrow, 2000). It is assumed that the physical system is close to the equilibrium state, and the distribution function deviates slightly from the local equilibrium distribution function and satisfies the following:

$$\begin{cases} \rho(x, t) = \sum_i f_i(x, t) = \sum_i f_i^{(0)}(x, t) \\ \rho u(x, t) = \sum_i e_i f_i(x, t) = \sum_i e_i f_i^{(0)}(x, t) \end{cases} \tag{15}$$

The Chapman-Enskog equation can be expressed as:

$$f_i = f_i^{(0)} + \varepsilon f_i^{(1)} + \varepsilon^2 f_i^{(2)} + \cdots \tag{16}$$

where $\varepsilon \ll 1$ is a small positive number, called the Knudsen number, which is the ratio of the average free path of particle motion to the length of macroscopic features. Moreover, ε^{-1} is equivalent to the size of the mesh, and the enforcing conditions are $\sum_i f_i^{(j)} = 0$, $\sum_i e_i f_i^{(j)} = 0$, $j \geq 1$.

Two types of time scales, $t_1 = \varepsilon t$ and $t_2 = \varepsilon^2 t$, and space scales, $x_1 = \varepsilon x$, are introduced. Further, the time and space derivatives are expanded on multiple scales as follows:

$$\frac{\partial}{\partial t} = \varepsilon \frac{\partial}{\partial t_1} + \varepsilon^2 \frac{\partial}{\partial t_2}, \frac{\partial}{\partial x} = \varepsilon \frac{\partial}{\partial x_1}. \tag{17}$$

$f_i(x + e_i \Delta t, t + \Delta t)$ can also be written as the Taylor expansion given below.

$$f_i(x + e_i \Delta t, t + \Delta t) - f_i(x, t) \\ = \Delta t \left(\frac{\partial}{\partial t} + e_i \cdot \frac{\partial}{\partial x} \right) f_i(x, t) \\ + \frac{1}{2!} \Delta t^2 \left(\frac{\partial}{\partial t} + e_i \cdot \frac{\partial}{\partial x} \right)^2 f_i(x, t) \\ = \frac{1}{3!} \Delta t^3 \left(\frac{\partial}{\partial t} + e_i \cdot \frac{\partial}{\partial x} \right)^3 f_i(x', t') \tag{18}$$

By comparing each order of the terms we have

$$\varepsilon : \left(\frac{\partial}{\partial t_1} + e_i \cdot \frac{\partial}{\partial x_1} \right) f_i^{(0)} = -\frac{1}{\tau \Delta t} f_i^{(1)}, \tag{19}$$

$$\varepsilon^2 : \frac{1}{2} \Delta t \left(\frac{\partial}{\partial t_1} + e_i \cdot \frac{\partial}{\partial x_1} \right)^2 f_i^{(0)} + \left(\frac{\partial}{\partial t_1} + e_i \cdot \frac{\partial}{\partial x_1} \right) f_i^{(1)} \\ + \frac{\partial}{\partial t_2} f_i^{(0)} = -\frac{1}{\tau \Delta t} f_i^{(2)}. \tag{20}$$

By substituting equation (19) into equation (20), equation (20) becomes

$$\left(\frac{1}{2} - \tau \right) \Delta t \left(\frac{\partial}{\partial t_1} + e_i \cdot \frac{\partial}{\partial x_1} \right)^2 f_i^{(0)} + \frac{\partial}{\partial t_2} f_i^{(0)} = -\frac{1}{\tau \Delta t} f_i^{(2)}. \tag{21}$$

According to equations (15) and (17), and taking the sum about i, equations (19) and (21) can be simplified as follows.

$$\frac{\partial}{\partial t_1} \sum_i f_i^{(0)} + \frac{\partial}{\partial x_1} \sum_i e_i f_i^{(0)} = 0, \tag{22}$$

$$\frac{\partial}{\partial t_2} \sum_i f_i^{(0)} + \left(\frac{1}{2} - \tau \right) \Delta t \left(\frac{\partial}{\partial t_1} \frac{\partial}{\partial x_1} \sum_i e_i f_i^{(0)} + \frac{\partial}{\partial x_1} \frac{\partial}{\partial x_1} \sum_i e_i e_i f_i^{(0)} \right) = 0 \tag{23}$$

From $\Sigma e_i \times$ equations (22) and (23) about i, we have

$$\frac{\partial}{\partial t_1} \sum_i e_i f_i^{(0)} + \frac{\partial}{\partial x_1} \sum_i e_i e_i f_i^{(0)} = 0 \tag{24}$$

$$\frac{\partial}{\partial t_2} \sum_i e_i f_i^{(0)} + \left(\frac{1}{2} - \tau \right) \Delta t \left(\frac{\partial}{\partial t_1} \frac{\partial}{\partial x_1} \sum_i e_i e_i f_i^{(0)} + \frac{\partial}{\partial x_1} \frac{\partial}{\partial x_1} \sum_i e_i e_i e_i f_i^{(0)} \right) = 0 \tag{25}$$

Equations (22)–(25) are multiscale equations obtained by CE expansion and multiscale analysis. To establish the Boltzmann grid equation of the water hammer, the one-dimensional space is discretised into segments with computational spacing $\Delta x = 1$. Then, equation (14) is transformed as follows based on the D1Q3 model.

$$f_i^{(0)} = A_i + B_i (e_i \cdot u) + C_i (e_i \cdot u)^2 + D_i |u|^2 \ (i = 0, 1, 2) \tag{26}$$

To simulate the water hammer with friction, an external force term is added to Boltzmann grid equation (11).

$$f_i(x + e_i \Delta t, t + \Delta t) - f_i(x, t) = -\frac{1}{\tau} [f_i(x, t) - f_i^{(0)}(x, t)] + R_i \tag{27}$$

In which

$$\sum_i R_i = -\frac{\mu'}{2D} v |v|, \sum_i e_i R_i = 0 \tag{28}$$

The Boltzmann grid method, like other CFD methods, has a similar relationship between the model of the equation and the actual flow field when actual problems are simulated. From the initial conditions and boundary conditions of the flow field to the initial conditions and boundary conditions of the model, the required parameters are calculated through the model and then converted to the corresponding parameters of the actual flow field according to the similarity relationship.

According to the similarity principle of fluid mechanics, to ensure the similarity between the calculated flow field

and the actual flow field, the Euler, Reynolds, Strouhal, and Froude numbers must be equal, that is,

$$\begin{cases} \lambda_{Eu} = \dfrac{\lambda_P}{\lambda_\rho \lambda_u{}^2} = 1 \\[2mm] \lambda_{Re} = \dfrac{\lambda_u \lambda_l}{\lambda_\nu} = 1 \\[2mm] \lambda_{St} = \dfrac{\lambda_l}{\lambda_t \lambda_u} = 1 \\[2mm] \lambda_{Fr} = \dfrac{\lambda_P}{\lambda_g \lambda_l} = 1 \end{cases} \tag{29}$$

For the above equations, the scale transformation relationship is as follows:

$$\lambda_x = \frac{L}{N}, \ \lambda_t = \frac{\lambda_x}{a}, \ \lambda_u = \frac{V}{v}, \ \lambda_h = \frac{H}{h} = \frac{a}{g}\lambda_u, \ \lambda_f = \frac{\mu}{\mu'} = \frac{1}{\lambda_t \lambda_u} \tag{30}$$

where L is the actual length of the pipe section; N is the number of pipe sections; λ_x, λ_t, λ_u, λ_h and λ_μ are the scales of space, time, flow rate, head of the pressure, and friction coefficient, respectively.

According to the continuity equation of fluids

$$\sum Q_{in} = \sum Q_{out} + Q_D. \tag{31}$$

The term Q_{in} is the discharge into the node, Q_{out} is the discharge out of the node, and Q_D is the demand for water at the node. The equality of hydraulic heads is

$$H_{P,I} = H_{P,J} = H_P \tag{32}$$

where I and J are pipe numbers. Substituting equation (30) into equations (31) and (32) the following equations can be derived.

$$\begin{cases} v_1\lambda_u A_1 + v_2\lambda_u A_2 = v_3\lambda_u A_3 + v_4\lambda_u A_4 + Q_D \\ h_1\lambda_h = h_2\lambda_h = h_3\lambda_h = h_4\lambda_h \end{cases} \tag{33}$$

or

$$\begin{cases} v_1 A_1 + v_2 A_2 = v_3 A_3 + v_4 A_4 + Q_D / \lambda_u \\ h_1 = h_2 = h_3 = h_4 \end{cases} \tag{34}$$

Then, putting equation (7) into equation (34) we have

$$\begin{cases} (f_{01} + f_{11} + f_{21})A_1 + (f_{02} + f_{12} + f_{22})A_2 \\ = (f_{03} + f_{12} + f_{23})A_3 + (f_{04} + f_{14} + f_{24})A_4 + Q_D / \lambda_u \\ f_{11} - f_{21} = f_{12} - f_{22} = f_{13} - f_{23} = f_{14} - f_{24} \end{cases} \tag{35}$$

$$\begin{cases} f_{21} = f_{11} + \dfrac{-(f_{01}+2f_{11})A_1 - (f_{02}+2f_{12})A_2 + (f_{03}+2f_{23})A_3 + (f_{04}+2f_{24})A_4 + Q_D/\lambda_u}{A_1+A_2+A_3+A_4} \\[2mm] f_{22} = f_{12} + \dfrac{-(f_{01}+2f_{11})A_1 - (f_{02}+2f_{12})A_2 + (f_{03}+2f_{23})A_3 + (f_{04}+2f_{24})A_4 + Q_D/\lambda_u}{A_1+A_2+A_3+A_4} \\[2mm] f_{13} = f_{23} + \dfrac{-(f_{01}+2f_{11})A_1 + (f_{02}+2f_{12})A_2 - (f_{03}+2f_{23})A_3 - (f_{04}+2f_{24})A_4 - Q_D/\lambda_u}{A_1+A_2+A_3+A_4} \\[2mm] f_{14} = f_{24} + \dfrac{-(f_{01}+2f_{11})A_1 + (f_{02}+2f_{12})A_2 - (f_{03}+2f_{23})A_3 - (f_{04}+2f_{24})A_4 - Q_D/\lambda_u}{A_1+A_2+A_3+A_4} \end{cases} \tag{36}$$

where the two digits, 1 and 2, in the subscripts of f indicate the upstream side of the node, while 3 and 4 indicate the downstream side of the node.

2.2 Basic boundary conditions

There are various elements (such as water tanks, pumps, various valves, and connecting fittings) in most water systems. Budinski (2016) provided a detailed presentation of some boundary conditions for the single-phase transition LBM. Therefore, the boundary conditions of the two-phase transient LBM are presented in the following section.

2.2.1 Downstream valve

Based on the orifice flow equation, the downstream valve conditions are deduced as

$$v = v_0 \phi \sqrt{\frac{h}{h_0}} \tag{37}$$

where ϕ is the hydraulic opening of the valve, and h_0 is the head of the reservoir. By substituting $v = f_0 + f_1 + f_2$ and $h = f_1 - f_2$ into the above equation, f_2 can be obtained.

$$f_2 = \left(-f_0 + f_1 + \frac{v_0^2 \phi^2}{2h_0}\right) + \sqrt{\left(f_0 + 2f_1 + \frac{v_0^2 \phi^2}{2h_0}\right)^2 - (f_0 + 2f_1)^2} \tag{38}$$

2.2.2 Upstream reservoir

The head of the upstream reservoir is assumed to be

$$H_0 = h_0 h_\lambda = \text{const} \tag{39}$$

where λ_h is a relevant parameter and $h_0 = f_1 - f_2$. Thus, $f_1 = h_0 + f_2$.

2.3 Two-phase transient flow based on DVCM

This study is focused on the two-phase transient flow without free air. The numerical calculation model uses multipoint to fix completely isolated cavities in the pipeline. The LBM can be iterated by supplying the boundary condition of cavities. Figure 2 shows the control volume in the pipe.

Figure 2 Control volume for continuity of vapour in the vapour zone
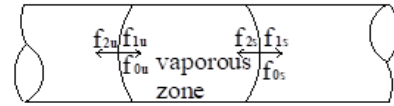
The distribution functions of upstream $(i - 1)$ point and downstream (i) point in the distributed vapour zones are provided by the following migration steps.

$$f_{1u}(i) = f_1(i-1), \ f_{0u} = f_0(i) \tag{40}$$

$$f_{2s}(i) = f_2(i+1), \ f_{0s} = f_0(i) \tag{41}$$

The pressure head of the cavity is equal to the vapour pressure head.

$$h = h_v \tag{42}$$

Then, $f_{2u}(i)$ and $f_{1s}(i)$ can be obtained.

$$f_{1s}(i) = h_v + f_{2s}(i) \qquad (43)$$

$$f_{2u}(i) = f_{1u}(i) - h_v \qquad (44)$$

The relationship between the local function and the velocity is given as:

$$v = f_2 + f_0 + f_1. \qquad (45)$$

Furthermore, during Δt, the volume of vapour is

$$VL = \sum (v_s - v_u) A\Delta t du \qquad (46)$$

where v_s and v_u are the velocities of the vapour cavity boundary.

When a cavity is near the closed valve at the downstream, $v_s = 0$, the volume of the vapour is given by:

$$VL = \sum -v_u A\Delta t du. \qquad (47)$$

3   Results and discussion

To validate the proposed LBM-DVCM model on more practical transition problems, the simulation results were compared with experimental tests carried out by Simpson (Simpson and Wylie, 1993), as shown in Figure 3.

The experimental device was a typical reservoir-pipevalve system composed of a copper straight and sloping pipe (with a length of 37.23 m, an internal diameter of 22.1 mm, and a pipe slope of 3.2°). The transient flows were caused by the rapid downstream valve closure. The wave speed was 1,319 m/s. The experimental results for two initial mean velocities of $V_0 = 0.3$ m/s and 1.4 m/s were used in this study, which are the pressure oscillations at the valve.

Water flowed from tank 1 to tank 2, and the closing time of the downstream valve was 0.006 s. The wave speed was 1319 m/s. The water level of tank 1, H_0, was a constant equal to 22 m. The fluid velocities (steady flow) V_0 were 0.3 m/s, 0.71 m/s, and 1.40 m/s.

Figure 3   Experimental apparatus layout
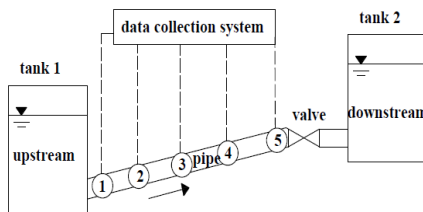
3.1   Verification of LBM-DVCM

Preliminarily, under the condition of rapid closing of the valve, the pressure oscillations at two different monitoring points were numerically generated (the valve and the midpoint of the pipeline). In this study, the grid number of the MOC-DVCM is $N_x = 16$ and the size is $\Delta x = L/N_x = 2.33$ m; however, the grid size of the LBMDVCM is $\Delta x = 1$ m. The comparison results at two different monitoring points of the LBM-DVCM, MOC-DVCM, and the experimental data

with velocities of 1.40 m/s, 0.71 m/s, and 0.3 m/s, are shown in Figure 4, Figure 5, and Figure 6, respectively.

Figure 4   Comparisons among the LBM-DVCM, MOC-DVCM, and experimental ($V_0 = 1.4$ m/s) results, (a) head at the valve, (b) head at the midpoint of pipe (see online version for colours)
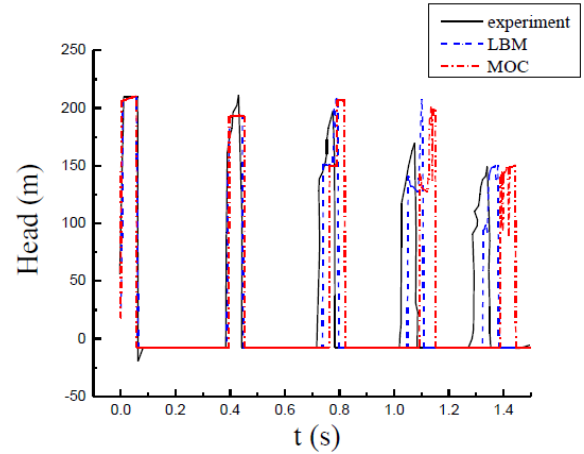
(a)
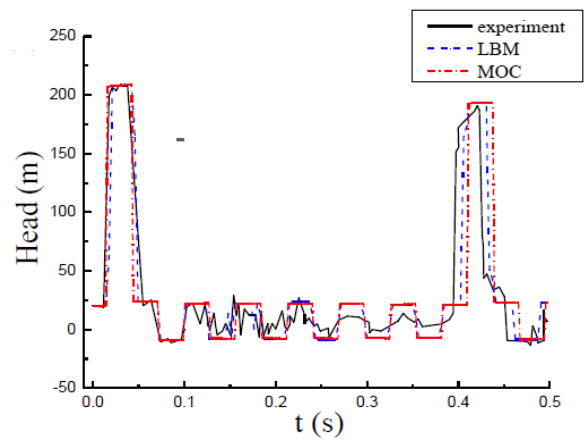
(b)

Figure 5   Comparisons among the LBM-DVCM, MOC-DVCM, and experimental ($V_0 = 0.7$ m/s) results, (a) head at the valve, (b) head at the midpoint of pipe (see online version for colours)
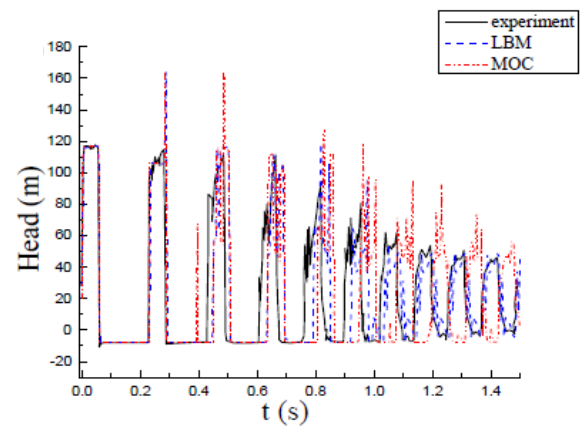
(a)

Figure 5 Comparisons among the LBM-DVCM, MOC-DVCM, and experimental ($V_0 = 0.7$ m/s) results, (a) head at the valve, (b) head at the midpoint of pipe (continued) (see online version for colours)

(b)
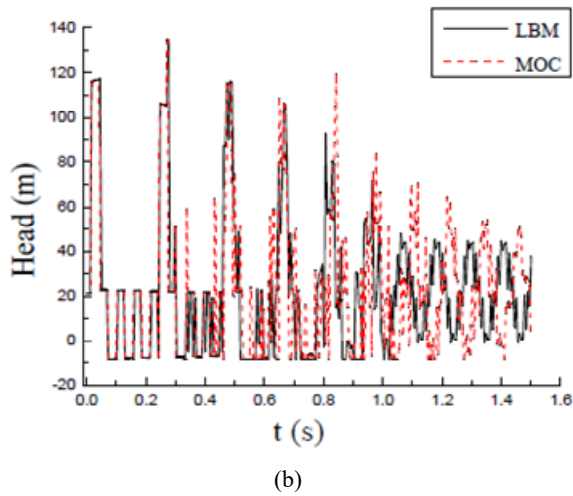
Figure 6 Comparisons among the LBM-DVCM, MOC-DVCM, and experimental ($V_0 = 0.3$ m/s) results, (a) head at the valve, (b) head at the midpoint of pipe (see online version for colours)

(a)

(b)
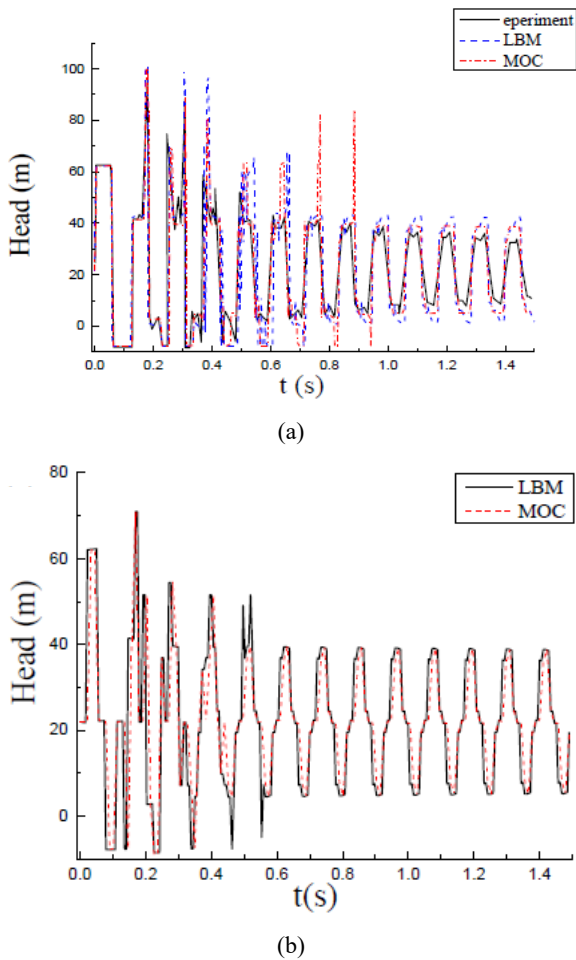
It is worth noting that both these two mathematical methods have high accuracy. When $V_0 = 1.4$ m/s, the first peak pressure heads at the valve are 210.04 m (experiment), 211.04 m (LBM-DVCM), and 210.23 m (MOC-DVCM),

respectively. In addition, the first peak pressure heads at the midpoint of the pipeline are 207.93 m (experiment), 209.80 m (LBM-DVCM), and 209.00 m (MOC-DVCM), respectively.

The rapid closure of the valve contributed to a Joukowsky pressure rise initially, and then the pressure was reduced to the vapour pressure, which resulted in pressure peaks owing to the collapse of the cavity. The pressure peaks predicted by the two models, as well as their shapes, almost coincide with the experimental data, and they are in good agreement with the experimental results.

Figure 7 Comparisons of the cavity volume between the MOC-DVCM and LBM-DVCM results ($V_0 = 1.4$ m/s), (a) at the valve, (b) at the middle point of the pipeline

(a)

(b)
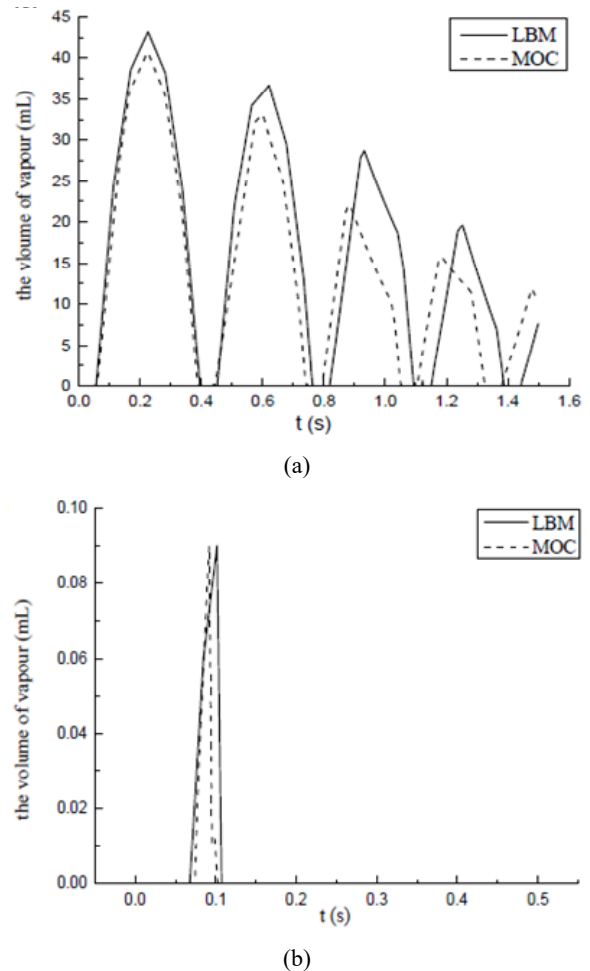
In Figures 4 and 5, the results of LBM-DVCM indicate insignificant time delay, although these two methods use the same frictional model which is the quasi-steady model. For the quasi-steady model, the turbulence state is updated at each time step, providing values for the instantaneous eddy viscosity as a function of the instantaneous velocity profile, as the wall shear stress is influenced by the velocity of the fluid (Wylie, 1985). Thus, the quasi-steady form is acceptable. In Figure 6, there are significant 'virtual pressure peaks' using MOC-DVCM, between 0.7 s to 1.0 s at the valve. Furthermore, at the two monitoring points, LBM-DVCM has fewer minor unrealistic pressure peaks regardless of the velocity; therefore, the MOC-DVCM is

more likely to produce unrealistic pressure peaks in the numerical simulation.

In terms of volume of vapour, LBM-DVCM and MOCDVCM are adopted to simulate the volume of cavity and its duration at three different fluid velocities, as shown in Figures 7–9. The volume and duration of the cavity are shown in Table 1, which provides detailed data about Figure 7.

Figure 8 Comparisons of the cavity volume between the MOC-DVCM and LBM-DVCM results ($V_0 = 0.7$ m/s), (a) at the valve, (b) at the middle point of the pipeline

(a)

(b)
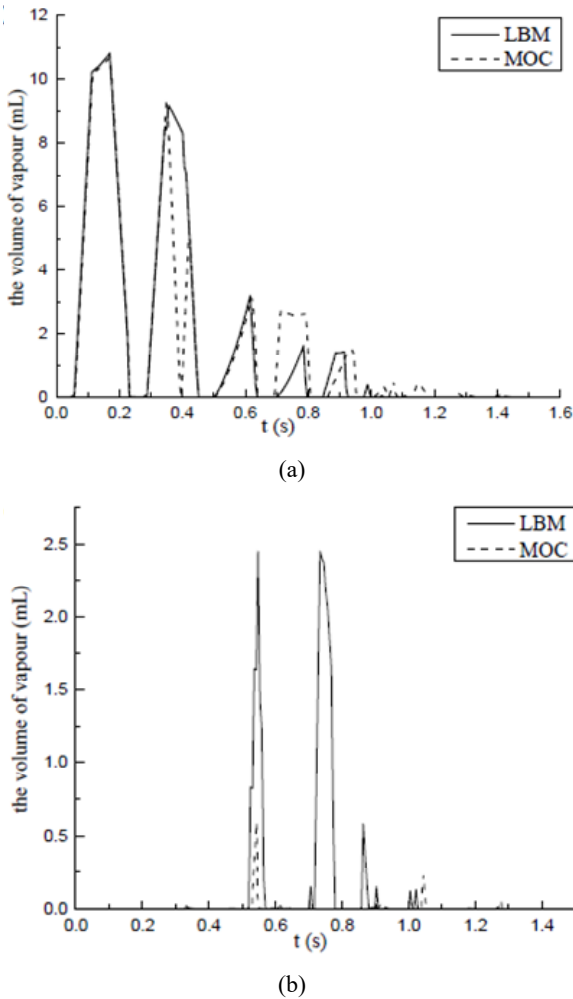
The duration of the cavity gets shorter and shorter owing to friction loss and energy dissipation. When the velocity of the fluid is 1.4 m/s, cavities appear in five periods near the valve. In this experimental data, it can be noted that the duration decreases after the first cavity is detected. At the same time, according to the simulation results, the cavities also disappeared eventually.

In the numerical results, the cavities near the valve are ten times bigger than the ones at the midpoint of the pipe, as shown in Figures 7–9. It can be observed that the higher the speed of the fluid, the bigger the cavities. Consequently, the lower the negative pressure, the greater the number and size of vapour cavities generated.

In the comparison, the two numerical results have a slight difference from the experimental data, particularly

when the fluid has a comparatively high speed. However, according to Table 1, LBM-DVCM is more accurate than MOCDVCM in terms of the appearance time of the cavity. There is an urgent need for experimental studies to establish more precise methods for determining accurate cavity volume.

Figure 9 Comparisons of the cavity volume between the MOC-DVCM and LBM-DVCM results ($V_0 = 0.3$ m/s), (a) at the valve, (b) at the middle point of the pipeline

(a)

(b)
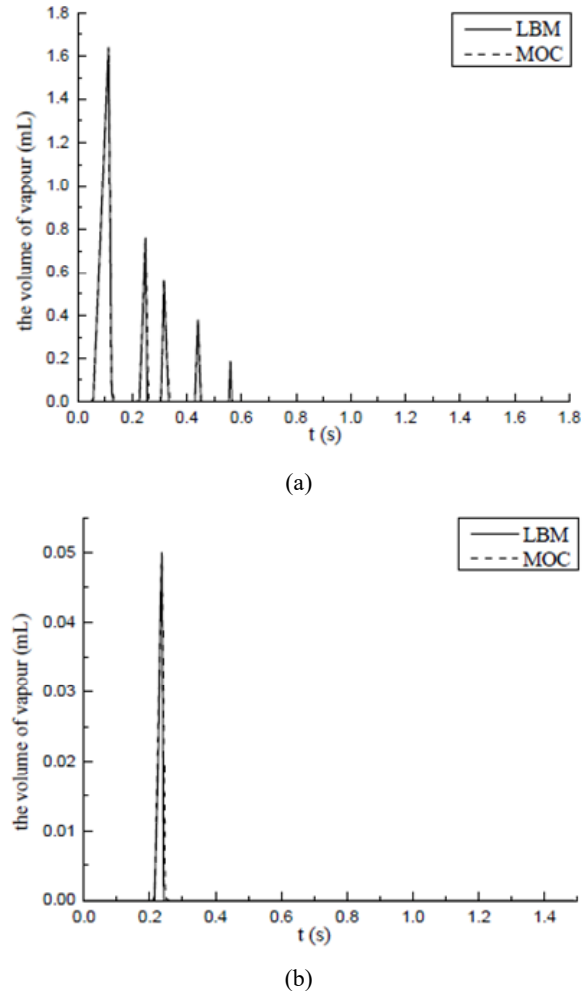
3.2 Practical pipeline system case study

To investigate the effect of the proposed LBM-DVCM in long-distance water supply systems, a practical case study of the water pipeline system was exhibited, which is the gravity flow section from the reservoir to the pump station (see Figure 10). The length of the pipeline was $L = 6,078$ m, the diameter was $D = 1.8$ m, the wave speed was $a = 867.9$ m/s, and the designed flow rate was $Q_0 = 6,875$ m³/h. Then, the hydraulic transient process period was $4L/a = 28$ s after quickly closing the valve or because of pump failure. The MOC-DVCM was applied to test the effect of the LBMDVCM in long-distance water supply systems owing to its widespread use in commercial software and the lack of experimental data. The pipe was divided into 61 segments, and the calculation time was $t_{max} = 1,200$ s in the simulation

In the numerical results, the first peak duration of the head at the valve is 0 to 14 s, and the maximum heads of the LBM-DVCM and MOC-DVCM are 104.09 m and 103.91 m, respectively. When the positive pressure wave generated by closing the valve is transmitted to the midpoint of the pipeline, the maximum heads of LBM-DVCM and MOCDVCM are 109.46 m and 109.37 m, respectively. In Figure 11, it can be observed that the two methods have a minimal difference in simulating the actual long water supply pipelines. Hence, the LBM-DVCM, like the MOC-DVCM, can be used in actual water supply projects.

Table 1 Volume and appearance time of the cavity

$V_0 = 1.4$ m/s		Volume of the cavity (m^3)	Duration time (s)
Valve	Experiment	——	0.0817–0.39421
		——	0.4417–0.7165
		——	0.7833–1.0192
		——	1.0841–1.2717
		——	1.3532–1.5
	MOCDVCM	4.282×10^{-5}	0.0677–0.3952
		3.627×10^{-5}	0.4629–0.7678
		3.167×10^{-5}	0.8355–1.1065
		2.135×10^{-5}	1.1742–1.4133
		——	1.4790–1.5
	LBMDVCM	4.367×10^{-5}	0.0621–0.3952
		3.703×10^{-5}	0.4573–0.7621
		2.704×10^{-5}	0.8242–1.0952
		2.019×10^{-5}	1.1573–1.3887
		——	1.4508–1.5
		——	0.074–0.097
Midpoint of the pipe	Experiment	——	0.074–0.097
	MOCDVCM	9.0×10^{-8}	0.074–0.099
	LBMDVCM	9.0×10^{-8}	0.074–0.099

Figure 10 Layout of the water supply system (the gravity flow section)
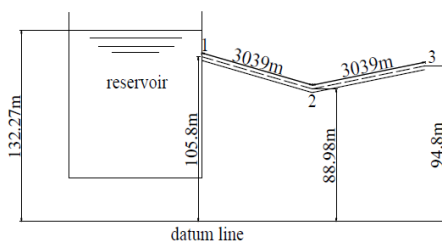
Table 2 Parameters of three points along the pipeline

Point	Elevation (m)	Piezometric head (m)	Free head (m)
1 (outlet of the reservoir)	105.8	132.270	26.470
2 (middle point of the pipe)	88.98	131.279	42.299
3 (valve)	94.8	130.327	35.527

Figure 11 Comparisons between the MOC-DVCM and LBM-DVCM results, (a) at the middle point of the pipeline, (b) at the valve

(a)

(b)
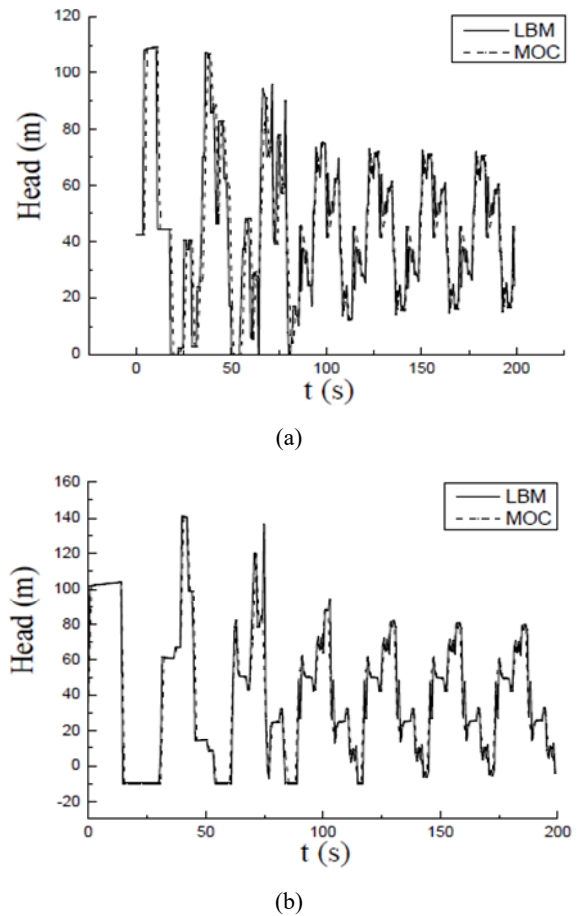
The short-time valve closing leads to significant pressure fluctuations at the valve; thus, the free head is easily reduced to the local vaporisation head (–9.8 m), and the water vaporises into the steam cavities. The middle point of the pipeline is conducive for preventing the vaporisation of water due to the lower elevation, and the water hammer pressure wave at the valve weakens because of the friction along the pipe.

It is worth noting that the calculation speed of the LBMDVCM was faster than that of the MOC, with the running time of approximately 8 s and 358 s, respectively, on a single i7 CPU and 8 GB RAM PC, thus making it possible to run eight analyses at once. However, the reason for this is beyond the scope of this paper.

4 Conclusions

In this study, based on the DVCM, a one-dimensional two phase transient flow numerical model was constructed using the LBM, and the following conclusions were obtained:

1 By comparing the experimental pressure data of the quick closing of the downstream valve in a simple reservoir-pipe-valve system, the LBM-DVCM has fewer minor unrealistic pressure spikes and insignificant phase lag, while both the LBM-DVCM

and the MOC-DVCM are accurate in predicting the peak pressures.

2   The LBM-DVCM is more accurate than the MOCDVCM in terms of the time of appearance of cavities and calculating the volume of air vapour.

3   In a practical long-distance water pipeline system, the LBM-DVCM has a good agreement with the MOCDVCM and runs faster.

In addition, the LBM-DVCM method can further be applied to viscoelastic pipelines and complex pipe networks, which will be the focus of future research.

Acknowledgements

References

Al-Neama, A.F., Kapur, N., Summers, J. et al. (2017) 'An experimental and numerical investigation of the use of liquid flow in serpentine microchannels for microelectronics cooling', *Appl. Therm. Eng.*, Vol. 116, pp.709–723, https://doi.org/10.1016/j.applthermaleng.2017.02.001.

Bergant, A. and Simpson, A.R. (1999) 'Pipeline column separation flow regimes', *Journal of Hydraulic Engineering-ASCE*, Vol. 125, pp.835–848, https://doi.org/10.1061/(asce)0733-9429(1999)125:8(835).

Bergant, A., Simpson, A.R. and Tijsseling, A.S. (2006) 'Water hammer with column separation: a historical review', *Journal of Fluids and Structures*, Vol. 22, pp.135–171, https://doi.org/10.1016/j.jfluidstructs.2005.08.008.

Budinski, L. (2016) 'Application of the LBM with adaptive grid on water hammer simulation', *Journal of Hydroinformatics*, Vol. 18, pp.687–701, https://doi.org/10.2166/hydro.2016.164.

Chen, S. and Doolen, G.D. (1998) 'Lattice Boltzmann method for fluid flows', *Annual Review of Fluid Mechanics*, Vol. 30, pp.329–364, https://doi.org/10.1146/annurev.fluid.30.1.329.

Cheng, Y., Zhang, S. and Chen, J. (1998) 'Water hammer simulation by the lattice Boltzmann method', *Shuili Xuebao/Journal of Hydraulic Engineering*, Vol. 29, No. 6, pp.25–31.

Cheng, Y-G. (1998) 'Water hammer simulation by the Lattice Boltzmann method', in Zhang, S.H. and Chen J.Z. (Eds.): *Transactions of the Chinese Hydraulic Engineering Society, J. Hydraul. Eng.*, pp.5–21.

Filippova, O. and Hanel, D. (1998) 'Grid refinement for lattice-BGK models', *Journal of Computational Physics*, Vol. 147, pp.219–228, https://doi.org/10.1006/jcph.1998.6089.

Frisch, U., Hasslacher, B. and Pomeau, Y. (1986) 'Lattice-gas automata for the Navier-stokes equation', *Phys. Rev. Lett.*, Vol. 56, pp.1505–1508, https://doi.org/10.1103/PhysRevLett.56.1505.

Gao, H., Tang, X., Li, X. et al. (2018) 'Analyses of 2D transient models for vaporous cavitating flows in reservoir-pipeline-valve systems', *Journal of Hydroinformatics*, Vol. 20, pp.934–945, https://doi.org/10.2166/hydro.2018.141.

Hoogerbrugge, P.J. and Koelman, J. (1992) 'Simulating microscopic hydrodynamic phenomena with dissipative particle dynamics', *Europhysics Letters*, Vol. 19, pp.155–160, https://doi.org/10.1209/0295-5075/19/3/001.

Sadafi, M., Riasi, A. and Nourbakhsh, S.A. (2012) 'Cavitating flow during water hammer using a generalized interface vaporous cavitation model', *Journal of Fluids and Structures*, Vol. 34, pp.190–201, https://doi.org/10.1016/j.jfluidstructs.2012.05.014.

Santoro, V.C., Crimi, A. and Pezzinga, G. (2018) 'Developments and limits of discrete vapor cavity models of transient cavitating pipe flow: 1D and 2D flow numerical analysis', *Journal of Hydraulic Engineering*, Vol. 144, https://doi.org/10.1061/(asce)hy.1943-7900.0001490.

Simpson, A.R. and Wylie, E.B. (1993) 'Large water-hammer pressures for column separation in pipelines-closure', *Journal of Hydraulic Engineering-ASCE*, Vol. 119, pp.144–145, https://doi.org/10.1061/(asce)0733-9429(1993)119:1(144).

Stewart, M., Walters T.W. and Wunderlich, G. (2018) *A Proposed Guideline For Applying Water hammer Predictions Under Transient Cavitation Conditions Part 2: Imbalanced Forces*, http://doi.org/10.1115/PVP2018-84339.

Wolf-Gladrow, D.A. (2000) 'Lattice-gas cellular automata and lattice Boltzmann models – introduction', *Lattice-Gas Cellular Automata and Lattice Boltzmann Models*, Vol. 1725, pp.1–13.

Wylie, E.B. (1985) 'Fundamental equations of water hammer-closure', *Journal of Hydraulic Engineering-ASCE*, Vol. 111, pp.1197–1200, https://doi.org/10.1061/(asce)0733-9429(1985)111:8(1197).

Wylie, E.B. (1992) 'Low void fraction two-component two-phase transient flow', in Bettess, R.W. and Watts, J. (Eds.): *Unsteady Flow and Fluid Transients*, pp.3–9, HR Wallingford, Durham, UK.

Zhang, C., Gong, J., Zecchin, A. et al. (2018) 'Faster inverse transient analysis with a head-based method of characteristics and a flexible computational grid for pipeline condition assessment', *Journal of Hydraulic Engineering*, Vol. 144, https://doi.org/10.1061/(asce)hy.1943-7900.0001438.

Zhou, L., Wang, H., Bergant, A. et al. (2018) 'Godunov-type solutions with discrete gas cavity model for transient cavitating pipe flow', *Journal of Hydraulic Engineering*, Vol. 144, https://doi.org/10.1061/(asce)hy.1943-7900.0001463.

Zhou, L., Wang, H., Liu, D. et al. (2017) 'A second-order finite volume method for pipe flow with water column separation', *Journal of Hydro-Environment Research*, Vol. 17, pp.47–55, https://doi.org/10.1016/j.jher.2016.11.004.

Zou, Q.S. and He, X.Y. (1997) 'On pressure and velocity boundary conditions for the lattice Boltzmann BGK model', *Physics of Fluids*, Vol. 9, pp.1591–1598, https://doi.org/10.1063/1.869307.

Nomenclature

A cross area of pipe (m^2)

A_i, B_i, C_i, D_i Lagrange's undetermined coefficients

a wave speed (m/s)

$C_k = (k = 1, 2, \cdots)$ undetermined constants

D pipe diameter (m)

E elastic modulus of the pipe wall material

e pipe-wall thickness (m)

e_i weight coefficients of the discrete velocity

F external force(N)

$f^{(0)}(x, v, t)$ local Maxwell-Boltzmann equilibrium distribution function

f_i particle distribution function along the i link

g gravitational acceleration (m/s2)

H piezometric head (m)

H_v vacuum pressure (m)

h_0 reservoir's water depth (m)

K bulk modulus of water

$K_{ij} = \partial\Omega_i/\partial f_j$ collision matrix

L length of pipe (m)

m molecular mass collision term

N number of sections of the pipe section

Q_{in} discharge into the node

Q_{out} discharge out of the node

Q_D demand for water at the node

R friction factor of the pipeline

s slip speed relative to the boundary (m/s)t = time (s)

u_w boundary speed(m/s)

V fluid (mixture) velocity (m/s)

V_0 initial velocity of pipeline(m/s)

VL volume of cavity (m3)

v velocity (m/s)

v_s downstream velocity of the cavity (m/s)

v_u upstream velocity of the cavity (m/s)

x spatial coordinate (m)

Greek symbols

$\alpha = w \to b$ direction from the outside of the boundary to the boundary

Δt time step of the iterative calculation (s)

Δx distance step of the iterative calculation (m)

ε Knudsen number

λ_h relevant parameter

λ friction factors

ρ density of water(kg/m3)

τ dimensionless relaxation time

τ_0 relaxation time of equilibrium state

ϕ hydraulic opening of the valve

$\Omega_i(f)$ collision term

$\omega = 1/\tau_0$ collision frequency